Journal of Controlled Release 328 (2020) 444–453

Contents lists available at ScienceDirect

Journal of Controlled Release

journal homepage: www.elsevier.com/locate/jconrel

Temperature-triggered micellization of interferon alpha-diblock copolypeptide conjugate with enhanced stability and pharmacology

Zhuoran Wang[a,b,c], Jianwen Guo[d], Xinyu Liu[a,b], Jiawei Sun[d], Weiping Gao[a,b,*]

[a] Department of Geriatric Dentistry, Beijing Laboratory of Biomedical Materials, Peking University School and Hospital of Stomatology, Beijing 100081, PR China
[b] Biomedical Engineering Department, Peking University, Beijing 100191, PR China
[c] CAS Engineering Laboratory for Nanozyme, Key Laboratory of Protein and Peptide Pharmaceutical, Institute of Biophysics, Chinese Academy of Sciences, Beijing 100101, PR China
[d] Department of Biomedical Engineering, School of Medicine, Tsinghua University, Beijing 100084, PR China

ARTICLE INFO

Keywords:
Protein-polymer conjugate
Polypeptide
Self-assembly
Protein delivery
Thermosensitivity

ABSTRACT

Polypeptides are useful in designing protein-polypeptide conjugates for therapeutic applications; however, they are not satisfactory in improving the stability of therapeutic proteins and extending their in vivo half-life. Here we show that thermally-induced self-assembly (TISA) of elastin-like polypeptide diblock copolymer fused interferon alpha (IFNα-ELP$_{diblock}$) into a spherical micelle can dramatically enhance the proteolytic stability of IFNα. Notably, the circulation half-life of IFNα-ELP$_{diblock}$ micelle (54.7 h) is 124.3-, 5.7-, and 1.4-time longer than those of free IFNα (0.44 h), freely soluble IFNα-ELP (9.6 h), and PEGylated IFNα (39.0 h), respectively. Importantly, in a mouse model of ovarian tumor, IFNα-ELP$_{diblock}$ micelle exhibited significantly enhanced tumor retention and antitumor efficacy over free IFNα, freely soluble IFNα-ELP, and even PEGylated IFNα. These findings provide a thermoresponsive supramolecular strategy of TISA to design protein-diblock copolypeptide conjugate micelles with enhanced stability and pharmacology.

1. Introduction

Therapeutic proteins are increasingly used in clinic for the treatment of various diseases [1,2]. Nevertheless, therapeutic proteins often possess short circulatory half-lives [3,4]. As a result, frequent administrations at high concentrations are required to maintain the therapeutically effective levels in blood, resulting in not only heavy financial burden and poor compliance of patient but also unsatisfactory therapeutic efficiency and serious side effects. Conjugating synthetic polymers like poly(ethylene glycol) (PEG) with therapeutic proteins to yield protein-polymer conjugates is the most frequently used strategy to prolong the circulatory half-lives [5–9]. So far, 16 PEGylated protein drugs have been permitted to be applied in clinic in the world [9]. However, PEGylation has some disadvantages that cannot be neglected [10]. Specifically, PEG itself does carry some potential safety risks, such as the antibody formation against PEG, hypersensitivity to PEG and vacuolation. Moreover, decreased activity and heterogeneity are also the negative aspects of PEGylated proteins, which may restrict the extensive use of PEGylated proteins.

Alternatively, polypeptides have recently been conjugated to protein drugs to elongate the circulation half-lives [9,11–14]. Unfortunately, due to the biodegradability, the circulation half-lives of protein-polypeptide conjugates (typically < 10 h) are substantially shorter than those of protein-polymer conjugates (typically > 30 h) [11–17]. As a prime example, interferon alpha (IFNα) is an important protein drug for the treatments of a wide range of viral and cancerous diseases mainly through its immunostimulatory functions [18,19], but it is unstable with a short circulation half-life [13–17]. Recently, different kinds of polypeptides have been conjugated to IFNα to improve the circulation half-life [13,14]. However, the half-lives of those polypeptides conjugated IFNα (6–10 h) are much shorter than those of PEG conjugated IFNα (PEGASYS, a Food and Drug Administration approved long-acting IFNα) (30–50 h) [15–17]. Hence, it is significant to overcome the limitations of protein-polypeptide conjugates in stability and circulation half-life.

Elastin-like polypeptides (ELPs) are a class of biocompatible, biodegradable, and thermosensitive biopolymers composed of Val-Pro-Gly-Xaa-Gly (VPGXG) repeats, in which the guest residual Xaa is any amino acids besides proline [20–26]. ELPs show inverse transition temperature (T_t), namely, they sharply phase separate to form coacervate in

* Corresponding author at: Department of Geriatric Dentistry, Beijing Laboratory of Biomedical Materials, Peking University School and Hospital of Stomatology, Beijing 100081, PR China.
E-mail address: gaoweiping@hsc.pku.edu.cn (W. Gao).

https://doi.org/10.1016/j.jconrel.2020.08.065
Received 14 June 2020; Received in revised form 27 August 2020; Accepted 31 August 2020
Available online 06 September 2020

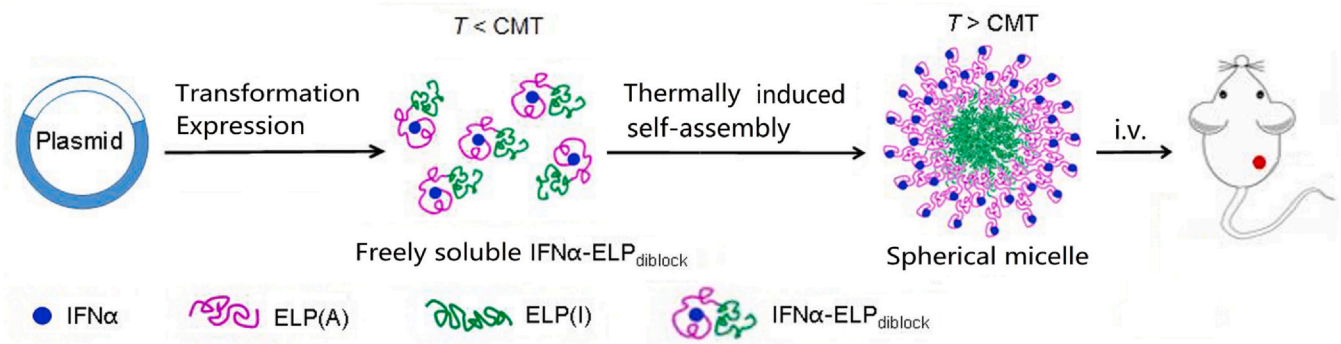

Scheme 1. Schematic illustration of thermally induced self-assembly of IFNα-$ELP_{diblock}$ into a spherical micelle with enhanced stability and retained bioactivity, leading to prolonged circulation half-life, increased tumor retention, and improved antitumor efficiency.

aqueous solution upon heating above their T_t. The phase separation is reversible in that the coacervate dissolves upon cooling the solution below the T_t. The T_t of ELPs can be finely tuned by changing the guest residue X in the pentapeptide repeat units and the number of repeat units (the chain length). More hydrophobic guest residues and longer chains mean that ELPs have lower T_t. An $ELP_{diblock}$ composed of two ELP blocks with different T_t values can self-assemble into a micelle above a critical micelle temperature (CMT), in which the hydrophobic ELP block desolvates to shape the micelle core and the hydrophilic ELP block forms the corona of the micelle [27–33]. $ELP_{diblock}$ has been fused to nanobodies to improve their receptor binding affinity through the mechanism of multivalency [34–36]. Nevertheless, to our knowledge, $ELP_{diblock}$ has not been used to improve the stability and circulation half-life of therapeutic proteins.

Herein we hypothesized that an IFNα-$ELP_{diblock}$ conjugate with a lower CMT than the body temperature would self-assemble into a micelle in which the closely packed IFNα-ELP chains in the corona of the micelle would be hard to be degraded by proteases due to the steric hindrance effect (Scheme 1). We further hypothesized that the micelle would circulate in blood for a prolonged time because of the improved proteolytic stability and the enlarged size of the micelle that can effectively reduce the renal clearance. The circulation half-life of IFNα-$ELP_{diblock}$ is as long as 54.7 h, which is more than 5 times longer than those (typically < 10 h) of the previously reported IFNα-polypeptide conjugates [11–14,37], especially which is 1.4 times longer than that of PEGASYS (39 h). As a result, in mice bearing ovarian tumors, the micelle exhibited remarkably increased antitumor efficacy without detectable side effects when compared with free IFNα, freely soluble IFNα-ELP, and even PEGASYS at the same dose.

2. Materials and methods

2.1. Construction of IFNα-$ELP_{diblock}$

The DNA sequence of IFNα-$ELP_{diblock}$ was synthesized and inserted into a pET-24a (+) vector for overexpression in *Escherichia coli* [37,38]. The details of gene synthesis, protein expression and purification were described in Supporting Information (Section 2.1).

2.2. Physicochemical characterization

The physicochemical properties of the protein samples were characterized using sodium dodecyl sulfate polyacrylamide gel electrophoresis (SDS-PAGE), matrix-assisted laser desorption/ionization time-of-flight mass spectrometry (MALDI-TOF-MS), circular dichroism (CD) spectra, photospectroscopy, dynamic light scattering (DLS), static light scattering (SLS), cryo-transmission electron microscopy (Cryo-TEM) and critical micelle concentration (CMC) of IFNα-$ELP_{diblock}$ was measured as described in Supporting Information (Section 2.2).

2.3. Thermoresponsive behaviours

The thermoresponsive behaviours of IFNα-$ELP_{diblock}$ as a function of temperature and concentration were measured by turbidimetric method as described previously [37].

2.4. Digestion with proteinase K

Digestion of IFNα-$ELP_{diblock}$ (1 mg/mL) with proteinase K at a molar ratio of 40:1 was conducted at 37 °C in 50 mM Tris-HCl, 2 mM $CaCl_2$, pH 8.0. After a certain incubation period (0, 0.5, 4, 8 h) at 37 °C, the proteolytic reaction was ceased by adding 0.03 M Phenylmethylsulfonyl fluoride (PMSF) in methanol. The digestion products were analyzed by SDS-PAGE, DLS and 3-(4,5-Dimethylthiazol-2-yl)-2,5-diphenyltetrazolium bromide (MTT) assay as described in Supporting Information (Section 2.3.2).

2.5. Digestion with serum

IFNα-$ELP_{diblock}$ (1 mg/mL) was incubated with mouse serum at 37 °C for 0, 1, 2, 3, 5 and 7 d. The antiproliferative activity of the digestion product was determined by MTT assay as described in Supporting Information (Section 2.3.3).

2.6. IFNα receptor (IFNαR) expression on OVCAR-3 cells

OVCAR-3 cells were fixed and then incubated with fluorescein isothiocyanate isomer I (FITC)-labelled IFNαR monoclonal antibody. The nucleus and membrane of the cells were stained with 4′,6-diamidino-2-phenylindole (DAPI) (Sigma) and wheat germ agglutinin (WGA) Alexa Fluor 594 (Invitrogen), respectively. Then the cells were visualized with a laser scanning confocal microscope of LSM710 (Carl Zeiss) and analyzed with a Zen_2012 software (blue edition).

2.7. IFNαR binding activity

After being incubated with Cy5-labelled IFNα-$ELP_{diblock}$, IFNα-ELP (A) and IFNα for 4 h with an IFNα concentration above (1 mg/mL) or below (0.4 μg/mL) the CMC of IFNα-$ELP_{diblock}$, the OVCAR-3 cells were fixed, stained, imaged and analyzed as described above. Mean optical density of Cy5 was quantified by Image J software.

2.8. Pharmacokinetics

IFNα-$ELP_{diblock}$ was injected intravenously into mice at 1 mg IFNα-equivalent/kg body weight (BW). Blood samples were taken at given time points and centrifuged to get plasma samples for measurements of the concentrations of the proteins in plasma as described in Supporting Information. Pharmacokinetic parameters were calculated using Drug

Analysis System 3.0 software.

2.9. Biodistribution

OVCAR-3 tumor-bearing mice received intravenous injection of 1.5 mg IFNα-equivalent/kg BW of IFNα-ELP$_{diblock}$. At 2, 48 and 120 h, the mice were executed and major tissues were harvested. The concentrations of IFNα equivalent in tissues were measured as described in Supporting Information (Section 2.4.2). After subtracting the background, the data were presented as IFNα equivalent (ng) per gram of tissue (ng/g tissue).

2.10. Antitumour efficacy

The animals bearing OVCAR-3 tumors of ~30 mm^3 in volume acquired intravenous injection of IFNα-ELP$_{diblock}$ at a dose of 1.5 mg IFNα-equivalent/kg BW once every week 4 times. Tumor volumes were evaluated via calipers every 3 days and calculated with the formula: volume = length × width^2 /2. The mice were weighed at the same time. When the tumor volumes were more than 300 mm^3 or the body weight loss was over 15%, the mice would be considered dead. To evaluate the biological safety, the mice were executed on the 15th day after intravenous injection. H&E staining and hematology analyses were performed as described in Supporting Information (Section 2.4.4).

2.11. Statistical analysis

Data are presented as mean ± standard error. Each group contains at least 3 independent repeats. The data were analyzed with one-way analysis of variance (ANOVA) test, which were followed by Tukey HSD test for multiple comparisons between different groups using SPSS software. Cumulative survival of mice was analyzed with Log-rank (Mantel-Cox) test. $P < 0.05$ was thought to be significant statistically. Statistical analyses were conducted with GraphPad Prism 5.0 software.

3. Results and discussion

3.1. Synthesis and physicochemical characterization

IFNα was genetically fused to the N-terminal of an ELP$_{diblock}$ of herein ELP(A)48-ELP(I)48, in which A (alanine) and I (isoleucine that is hydrophobic relative to alanine) in parenthesis are the guest residues of the hydrophilic ELP(A)48 block and the hydrophobic ELP(I)48 block, respectively (Scheme 1). The repeat unit number of ELP(A)48 was designed to be 48, which is the same as that of ELP(I)48. Meanwhile, a control sample of IFNα-ELP(A) was constructed. The repeat unit number of ELP(A) was 96, which is the same as the sum of the repeat unit numbers of ELP(A)48 and ELP(I)48 in IFNα-ELP$_{diblock}$, so that the molecular sizes of IFNα-ELP$_{deblock}$ and IFNα-ELP(A) are almost the same. The conjugates were biosynthesized and purified through inverse transition cycling [13], as indicated by SDS-PAGE in which a single band for each conjugate was seen with the expected molecular weight (Fig. 1A). MALDI-TOF-MS was further used to determine the accurate molecular weights of IFNα-ELP$_{diblock}$, IFNα-ELP(A) and free IFNα to be 58219.5, 56204.0, and 20338.6 Da, respectively (Fig. 1B), which well matched with the theoretical ones of 58221.7, 56201.9, and 20340.1 Da, respectively. The CD shape and peak intensity of IFNα-ELP$_{diblock}$ and IFNα-ELP(A) were found to be nearly identical to those of IFNα, indicating that the site-specific conjugation to ELPs did not alter the secondary structure of IFNα (Fig. 1C).

The thermally responsive behaviours of IFNα-ELP$_{diblock}$ and IFNα-ELP(A) were studied with turbidimetric assay (Fig. 1D). IFNα-ELP(A) underwent a first-order phase transition of unimer-to-aggregate when the solution was heated above its T_t, as indicated by a dramatic increase in the solution turbidity over a 1–2 °C temperature span. As expected, the T_t is concentration dependent and well above the body temperature of 37 °C, as indicated by the increase in T_t with the decrease in concentration (Fig. 1E and Fig. S1). By contrast, IFNα-ELP$_{diblock}$ showed a two-step thermoresponsive phase transition; namely, the solution was transparent at low temperatures (< 21 °C), but the turbidity increased with the temperature in the range of 21–50 °C (Fig. 1D). Upon further heating, the turbidity increased dramatically and plateaued in the range of 51–72 °C. The two-step change in turbidity could be attributed to unimer-to-micelle and micelle-to-coacervate transitions, which was previously observed in ELP$_{diblock}$ systems [27]. The first small increase in turbidity was indicative of the formation of micelle, which was effected by the thermoresponsive phase transition for the ELP(I)48 block with a low T_{t1} of 20 °C. T_{t1} is the temperature where the optical density (OD) value first deviates from the baseline. When the solution was heated above 50 °C, the ELP(A)48 block underwent its thermoresponsive phase transition with a high T_{t2}, inducing the production of large aggregates as suggested by the high value in OD. T_{t2} is the maximum temperature in the derivative of OD to temperature. The concentration dependence of T_{t1} and T_{t2} was further investigated for IFNα-ELP$_{diblock}$ (Fig. 1E and Fig. S2). The T_{t1} increased with the decrease of concentration of IFNα-ELP$_{diblock}$ but was well below the body temperature of 37 °C even at low concentrations, suggesting the high integrity of the micelle in vivo. In contrast, the T_{t2} was almost independent of concentration, presumably due to the high local ELP(A)48 concentration in the corona that was caused by the close packing of IFNα-ELP(A)48 chains in the corona of the micelle.

Next, the temperature-induced self-assembly of IFNα-ELP$_{diblock}$ at a concentration of 25 μM was investigated by DLS (Fig. 1F). The unimer of IFNα-ELP$_{diblock}$ (hydrodynamic radius (R_h) = 8.5 nm) formed monodisperse micelle (R_h = 25.5 nm) at a critical micelle temperature (CMT) of 21 °C that was close to the T_{t1}. The micelle was stable up to 50 °C, followed by the formation of bulk aggregates due to the phase transition of the corona block. As expected, the unimer of IFNα-ELP(A) (R_h = 9.6 nm) formed bulk aggregates when heated above the T_t of 58 °C. To further characterize the structure of IFNα-ELP$_{diblock}$, SLS was applied to determine the radius of gyration (R_g = 17.4 nm) (Table S1). The $\rho = R_g/R_h$ ratio was further determined to be 0.74 that is close to the theoretical one of 0.775 for homogeneous hard spheres [39], suggesting that the morphology of IFNα-ELP$_{diblock}$ micelle was spherical. Indeed, Cryo-TEM revealed uniform nanospheres with a size of 48 nm in diameter (Fig. 1G). The CMC of IFNα-ELP$_{diblock}$ at 37 °C was determined to be as low as 0.5 μg IFNα/mL in PBS and 0.3 μg IFNα/mL in mouse serum (Fig. S3). The low CMC and enlarged R_h (25.5 nm) suggest that the micelle would circulate in blood with the integrated micellar structure for a prolonged time due to the reduced renal clearance as compared to IFNα-ELP(A) (R_h = 9.6 nm) and IFNα (R_h = 2.8 nm) (Fig. 1H).

3.2. IFNα receptor (IFNαR) binding activity and antiproliferative characterization

IFNαR is highly expressed on human ovarian tumor cells (OVCAR-3) (Fig. 2A). To study the IFNαR binding activity of IFNα-ELP$_{diblock}$, OVCAR-3 cells were incubated with cyanine 5 (Cy5)-labelled IFNα-ELP$_{diblock}$ for 4 h at an IFNα concentration above or below the CMC of IFNα-ELP$_{diblock}$ (Fig. 2B and C). When the IFNα concentration was lower than the CMC, the IFNαR binding activity of IFNα-ELP$_{diblock}$ unimer was close to that of IFNα-ELP (A) as indicated by the similar Cy5 fluorescence intensities in the cells, but was lower than that of IFNα as implied by the weaker Cy5 fluorescence in the cells treated with the IFNα-ELP$_{diblock}$ unimer than IFNα. On the other hand, when the IFNα concentration was higher than the CMC, the IFNαR binding activity of IFNα-ELP$_{diblock}$ micelle was lower than that of IFNα-ELP (A) as indicated by the weaker Cy5 fluorescence in the cells treated with IFNα-ELP$_{diblock}$ micelle than IFNα-ELP(A), probably due to the steric hindrance caused by the close packing of IFNα-ELP(A)48 chains, a part of IFNα-ELP(A)48-ELP(I)48, in the corona of the IFNα-ELP$_{diblock}$

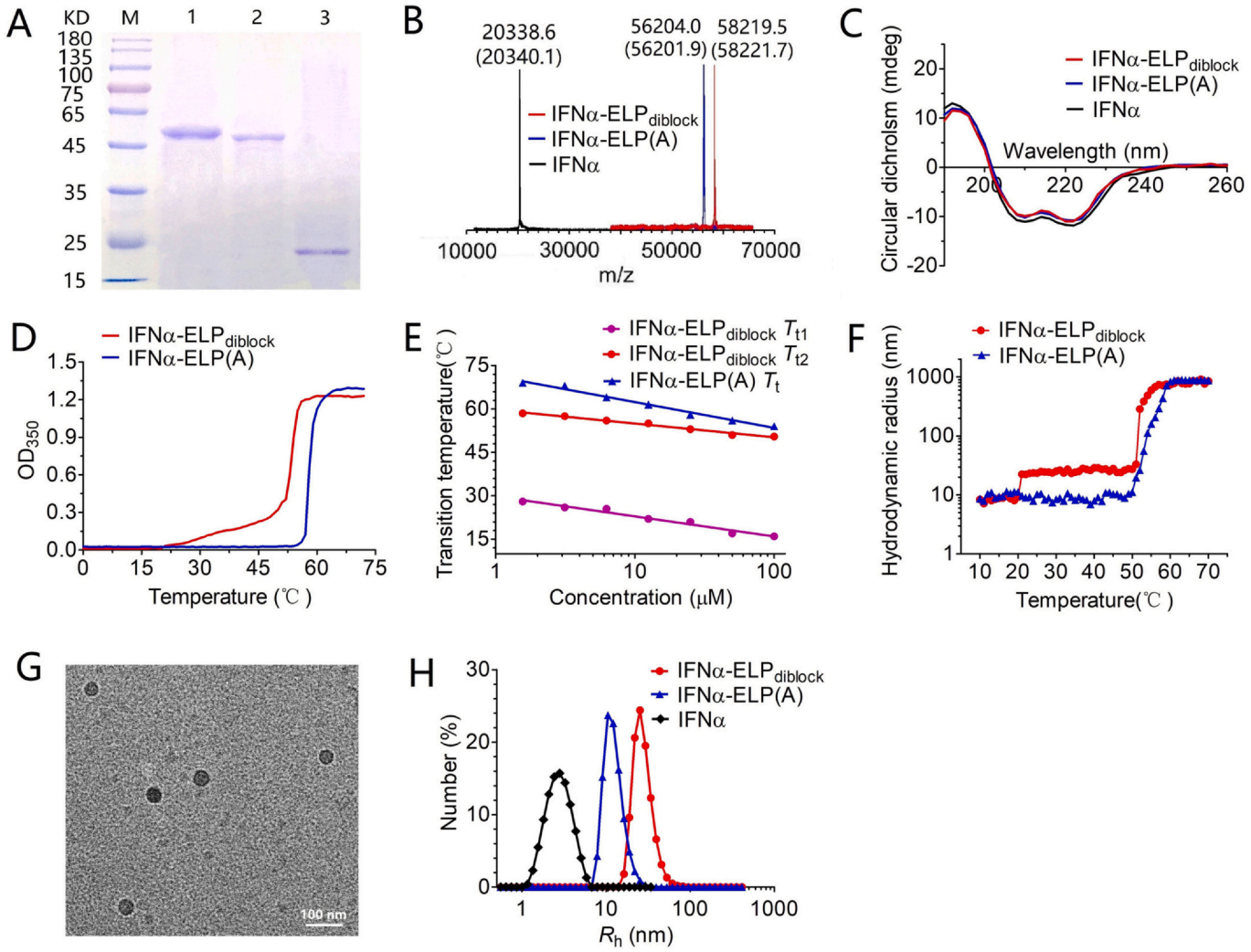

Fig. 1. Physicochemical characterization of IFNα-ELP$_{diblock}$. (A) SDS-PAGE analyses of IFNα-ELP$_{deblock}$, IFNα-ELP(A) and IFNα after purification. M: marker, Lane 1: IFNα-ELP$_{diblock}$, lane 2: IFNα-ELP(A), lane 3: IFNα. (B) MALDI-TOF-MS spectra of IFNα-ELP$_{deblock}$, IFNα-ELP(A) and IFNα. In parenthesis, the theoretical mass of each sample is given. (C) CD spectra. (D) Turbidity (OD_{350}) of IFNα-ELP$_{diblock}$ and IFNα-ELP(A) at 25 μM in PBS versus temperature. (E) The concentration dependence of T_t. (F) R_h of IFNα-ELP$_{diblock}$ and IFNα-ELP(A) at 25 μM in PBS versus temperature. (G) Cryo-TEM analysis of IFNα-ELP$_{diblock}$ micelle. (H) DLS analyses.

micelle. Taken together, these data suggest that multivalent effect did not exist in this system or was so weak that it could be compromised by the decreased IFNαR binding activity of the micelle, which is consistent with our previous observation in another micelle system [17,40]. Notably, cross-linking of IFNα receptors is not required for signal transduction [41], which means that multivalent effect should be weak if existing in this system.

Next, we tested the in vitro antiproliferative activity of IFNα-ELP$_{diblock}$ using OVCAR-3 cells (Fig. 2D). All the IFN analogues did not show any cytotoxicity to OVCAR-3 cells even if the IFNα concentration was as high as 10^7 pg/mL, indicating OVCAR-3 cells are insensitive to the IFNα analogues. Nevertheless, this result did not mean that the IFNα analogues would be ineffective in killing OVCAR-3 cells in vivo considering that IFNα mainly functions by stimulating anticancer immune response [19]. Therefore, Daudi cells that are highly sensitive to IFNα were further used for in vitro antiproliferative activity evaluation (Fig. 2E). The antiproliferative activity of IFNα-ELP$_{diblock}$ (half maximal inhibitory concentration (IC50) = 61.6 pg IFNα/mL) was similar to that of IFNα-ELP(A) (IC50 = 60.4 pg IFNα/mL), which was 35.2% of that for IFNα (IC50 = 21.7 pg IFNα-equivalent/mL). Notably, the antiproliferative activities of IFNα-ELP$_{diblock}$ and IFNα-ELP(A) were 5.7- and 5.8-time higher than that for PEGASYS (IC50 = 350.6 pg IFNα/mL), respectively, indicating that these ELP conjugations were substantially superior to PEGylation in activity retention.

3.3. Proteolytic stability

To study the proteolytic stability of IFNα-ELP$_{diblock}$ micelle, it was treated with protease K at 37 °C and then analyzed by SDS-PAGE (Fig. 3A). Much longer incubation time was needed to digest IFNα-ELP$_{diblock}$ micelle than IFNα and IFNα-ELP(A), which indicates that IFNα-ELP$_{diblock}$ micelle was much more resistant to proteolysis than IFNα and IFNα-ELP(A). This result was corroborated by DLS analysis (Fig. 3B). Only one single peak with a R_h of 23.6 nm was observed after the incubation for 4 h, which well overlapped that for IFNα-ELP$_{diblock}$ before the incubation, indicating that IFNα-ELP$_{diblock}$ micelle was structurally stable against proteolysis. On the contrary, multiple species with lower R_h values were observed for IFNα-ELP(A) after the incubation for 4 h, suggesting that IFNα-ELP(A) was degraded into small species. IFNα was completely digested into very small species, as indicated by a single peak with a very small R_h of 0.51 nm. These data indicate that IFNα-ELP(A) and IFNα were structurally unstable against proteolysis. We further found that the structural stability was correlated with the functional stability. The antiproliferative activity of IFNα-ELP$_{diblock}$ micelle decreased much more slowly with the time of incubation with protease K than those of IFNα and IFNα-ELP(A) (Fig. 3C).

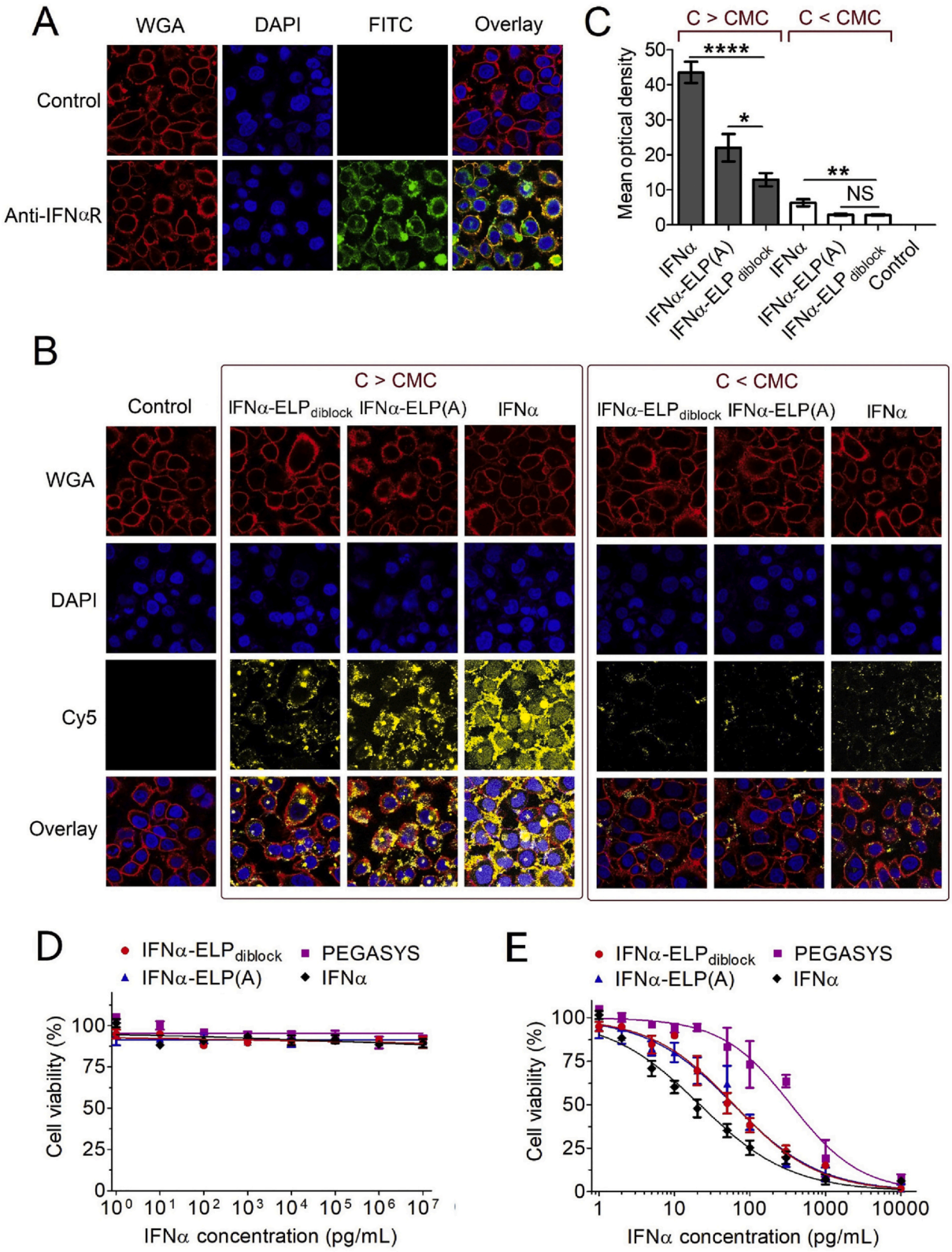

Fig. 2. IFNαR binding and antiproliferative activities of IFNα-ELP$_{diblock}$. (A) Immunofluorescence staining of OVCAR-3 cells to show membrane localization of IFNαR. The cell membrane is stained with WGA in red; the cell nucleus is stained with DAPI in blue; FITC-labelled IFNαR monoclonal antibody is in green. (B) Localization of Cy5-labelled IFNα-ELP$_{diblock}$, IFNα-ELP(A) and IFNα on OVCAR-3 cells after incubation for 4 h at an IFNα concentration above (1 mg/mL) or below (0.4 μg/mL) the CMC of IFNα-ELP$_{diblock}$. Cy5-labelled IFNα-ELP$_{diblock}$, IFNα-ELP(A) and IFNα are in yellow. (C) Mean optical density of Cy5 quantified from panel B by Image J software, which reflects the IFNαR binding activity of IFNα-ELP$_{diblock}$, IFNα-ELP(A) or IFNα ($n = 3$, $^{*}P < 0.05$, $^{**}P < 0.01$, $^{****}P < 0.0001$). (D) Cytotoxicity against OVCAR-3 cells ($n = 3$). (E) Cytotoxicity against Daudi B cells ($n = 3$). (For interpretation of the references to colour in this figure legend, the reader is referred to the web version of this article.)

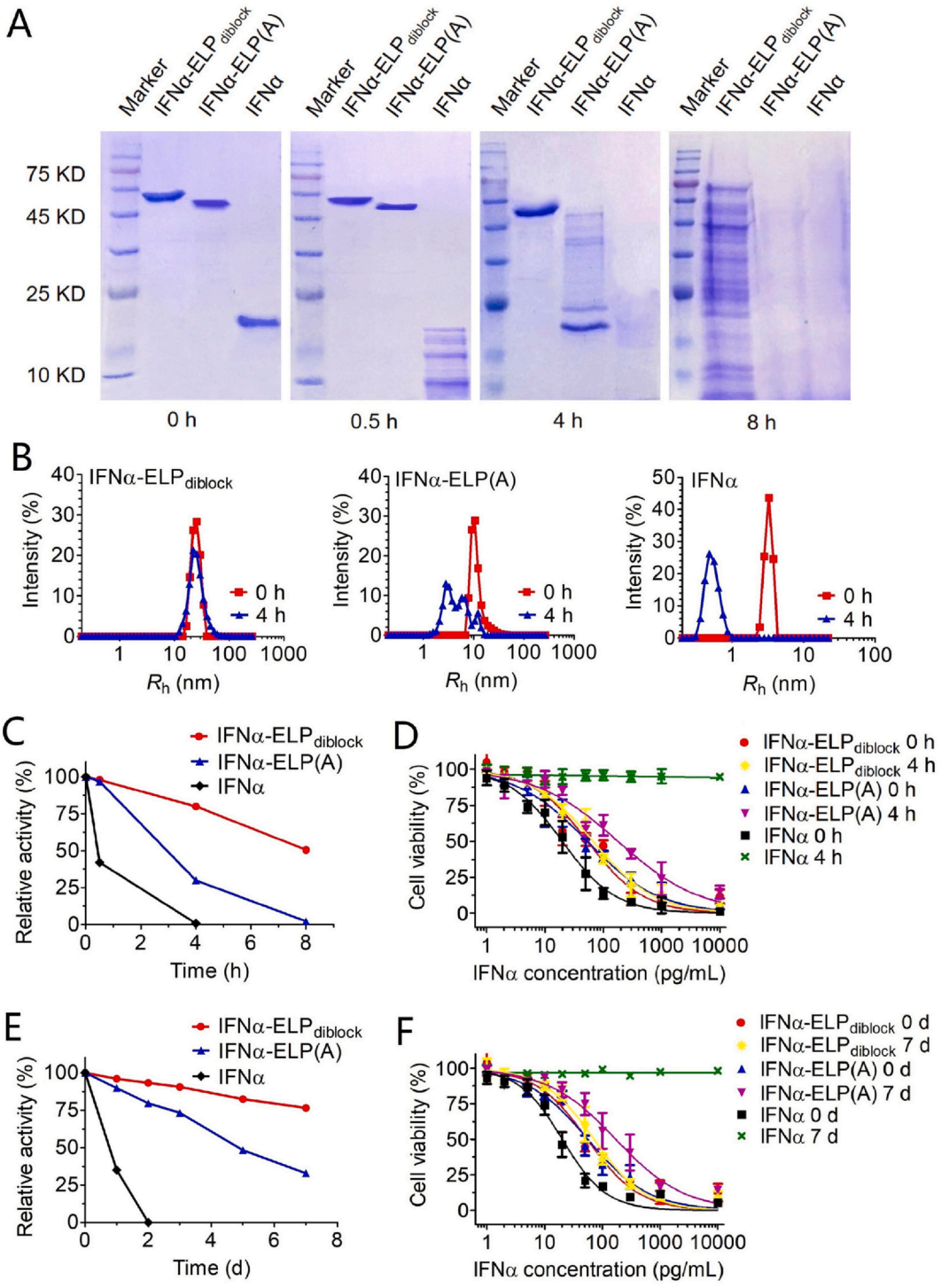

Fig. 3. Proteolytic stability of IFNα-ELP$_{diblock}$. (A) SDS-PAGE analysis of IFNα-ELP$_{diblock}$ digested with proteinase K at given time points at 37 °C. M: marker, lane 1: IFNα-ELP$_{diblock}$, lane 2: IFNα-ELP(A), lane 3: IFNα. (B) DLS analysis of IFNα-ELP$_{diblock}$ incubated with proteinase K for 0 and 4 h. (C) The antiproliferative activity retention versus the time of incubation with protease K. (D) The antiproliferative activity measurements after the incubations with protease K for 0 h and 4 h. (E) The antiproliferative activity retention versus the time of incubation with serum at 37 °C. (F) The antiproliferative activity measurements after the incubations with serum for 0 d and 7 d (n = 3).

Specifically, the antiproliferative activity of IFNα-ELP$_{diblock}$ micelle (IC50 = 66.9 pg IFNα/mL) was 2.6-time higher than that of IFNα-ELP (A) (IC50 = 178.1 pg IFNα/mL) after the incubation with protease K for 4 h (Fig. 3D). IFNα almost completely lost its activity after the 4 h incubation. These data indicate that IFNα-ELP$_{diblock}$ micelle was much more stable, in function, against proteolysis than IFNα-ELP(A) and IFNα. This result was further supported by incubating these samples with serum at 37 °C. The antiproliferative activity of IFNα-ELP$_{diblock}$ decreased much more slowly with the time of incubation with serum than those of IFNα and IFNα-ELP(A) (Fig. 3E). The antiproliferative activity of IFNα-ELP$_{diblock}$ (IC50 = 71.5 pg IFNα/mL) was 2.4-time higher than that of IFNα-ELP(A) (IC50 = 170.3 pg IFNα/mL) after the incubation with serum for 7 d (Fig. 3F). IFNα completely lost the activity after the incubation. The improvements in the structural and

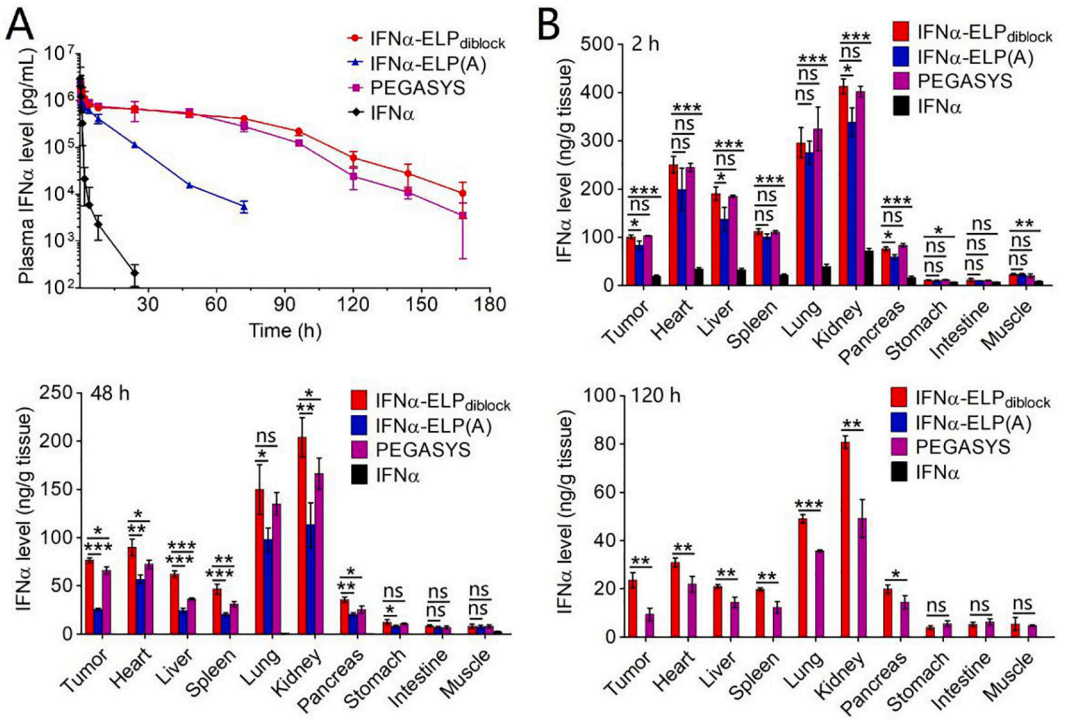

Fig. 4. Pharmacokinetic profile and biodistribution of IFNα-ELP$_{diblock}$. (A) Plasma IFNα concentration as a function of time post intravenous injection. (B) IFNα levels in tumors and major tissues at 2, 48 and 120 h post intravenous injection (n = 3). $^{*}P < 0.05$, $^{**}P < 0.01$, $^{***}P < 0.001$, considerable difference for IFNα-ELP$_{diblock}$ relative to other groups.

functional stabilities of IFNα-ELP$_{diblock}$ micelle against protease K and serum over IFNα-ELP(A) and IFNα could be attributed to the compact packing of the IFNα-ELP(A)48 block in the corona of the micelle. The resulting steric hindrance could hamper the interactions between the IFNα-ELP(A)48 chains and proteases and thus effectively reduce the enzymatic degradation of IFNα-ELP$_{diblock}$.

3.4. Pharmacokinetics and biodistribution

The pharmacokinetics of IFNα-ELP$_{diblock}$ was evaluated after intravenous bolus injection in a mouse model (Fig. 4A). After intravenous bolus injection, the plasma level of IFNα rapidly dropped, with a short distribution half-life ($t_{1/2\alpha}$) of 0.07 h and a short terminal half-life ($t_{1/2\beta}$) of 0.44 h (Table S2). By contrast, the plasma IFNα concentrations of IFNα-ELP$_{diblock}$, IFNα-ELP(A), and PEGASYS slowly decreased with time, with prolonged $t_{1/2\alpha}$ and $t_{1/2\beta}$. Notably, the $t_{1/2\alpha}$ of IFNα-ELP$_{diblock}$ (1.1 h) was 16.9-, 2.9-, and 1.4-time longer than those of IFNα (0.07 h), IFNα-ELP(A) (0.38 h), and PEGASYS (0.78 h), respectively. The $t_{1/2\beta}$ of IFNα-ELP$_{diblock}$ (54.7 h) was 124.3-, 5.7-, and 1.4-time longer than those of IFNα (0.44 h), IFNα-ELP(A) (9.6 h), and PEGASYS (39.0 h), respectively. Consequently, the area under the curve (AUC) of IFNα-ELP$_{diblock}$ (63.2 mg/L·h) was 48.6-, 5.2-, and 1.3-time larger than those of IFNα (1.3 mg/L·h), IFNα-ELP(A) (12.1 mg/L·h), and PEGASYS (50.5 mg/L·h), respectively. This dramatically improved pharmacokinetics demonstrates that IFNα-ELP$_{diblock}$ was much more effectual in meliorating the pharmacokinetic profile of IFNα than IFNα-ELP(A), which could be attributed to the enlarged size and enhanced stability of IFNα-ELP$_{diblock}$ micelle over IFNα-ELP(A). More interestingly, the pharmacokinetics of IFNα-ELP$_{diblock}$ was even better than that of PEGASYS, due to the larger size of the IFNα-ELP$_{diblock}$ mecelles (Fig. S4).

The distribution of IFNα-ELP$_{diblock}$ in major tissues was examined in a nude mouse model of ovarian tumor (Fig. 4B). Notably, the IFNα concentration of IFNα-ELP$_{diblock}$ in tumor (23.5 ng IFNα/g tissue) was 2.5-time higher than that of PEGASYS (9.5 ng IFNα/g tissue) at 120 h after intravenous injection, whereas the IFNα concentrations of IFNα and IFNα-ELP(A) approached zero. More IFNα-ELP$_{diblock}$, IFNα-ELP(A), PEGASYS, and IFNα were detected in kidney than in other tissues, suggesting that they could be removed from the body via renal clearance. Also, the concentrations of them in lung were found high, presumably due to the high levels of IFNα receptors distributed in lung [41]. Collectively, these results demonstrate that IFNα-ELP$_{diblock}$ was much more effective than IFNα-ELP(A) and even better than PEGASYS in enhancing the tumor retention of IFNα, and existed in tumor in the form of unimer.

3.5. Antitumor efficacy

We reasoned that the significantly enhanced pharmacokinetic property and tumor retention of IFNα-ELP$_{diblock}$ over IFNα-ELP(A), PEGASYS, and IFNα would translate into remarkably improved antitumor efficacy. In a nude mouse model of ovarian tumor with a size of 30 mm^3 in volume, IFNα-ELP$_{diblock}$, IFNα-ELP(A), PEGASYS, and IFNα were intravenously injected at the same dose (Fig. 5A). Notably, IFNα-ELP$_{diblock}$ was extraordinarily more effective than IFNα-ELP(A) in inhibition of tumor growth (Fig. 5B, Fig. S5 and S6), due to the substantially improved pharmacokinetics and tumor retention. Furthermore, IFNα-ELP$_{diblock}$ exhibited much higher potency in suppressing tumor growth than PEGASYS, due to the high activity retention and the improved pharmacokinetics and tumor retention. By contrast, IFNα was almost ineffective in inhibition of tumor growth, due to its poor pharmacokinetics and tumor retention. Specifically, at 40 d after treatment, the average tumor size for the IFNα-ELP$_{diblock}$ treatment (68.4 mm^3) was 13.9-, 7.4-, and 3.3-time smaller than those for the IFNα (950.0 mm^3), IFNα-ELP(A) (505.5 mm^3), and PEGASYS (228.9 mm^3) treatments, respectively. Correspondingly, the animal survival rates for the IFNα-ELP$_{diblock}$, IFNα-ELP(A), PEGASYS, and IFNα treatments were 40% (tumor free), 0%, 10% (tumor free), and 0%, respectively. The improved proteolytic stability, the enlarged size, and the reduced binding activity of the IFNα-ELP$_{diblock}$ micelle can effectively prolong

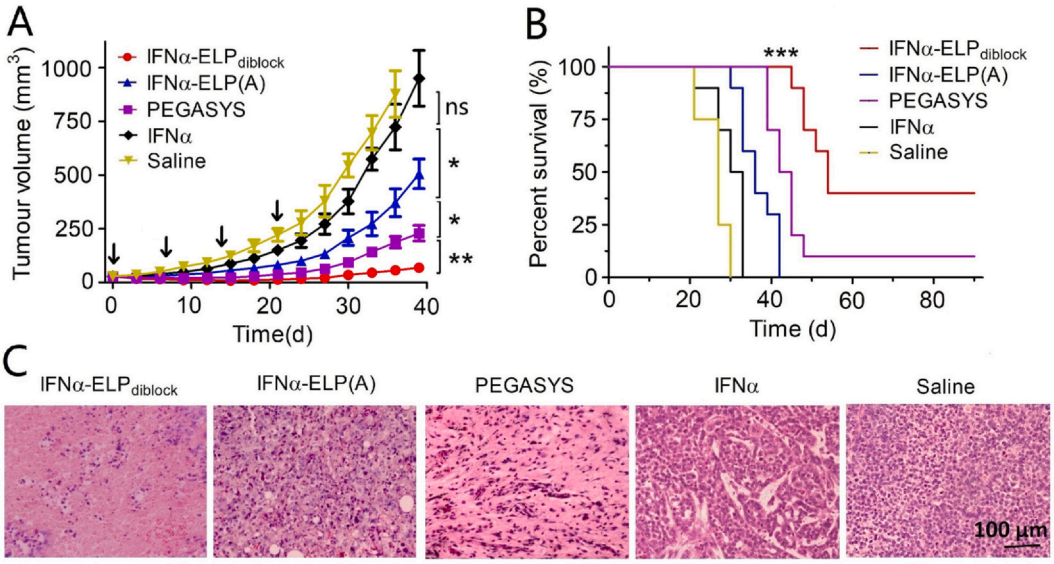

Fig. 5. Antitumor efficacy of IFNα-ELP$_{diblock}$. (A) Suppression of ovarian tumor growth after intravenous injections with IFNα-ELP$_{diblock}$, IFNα-ELP(A), PEGASYS and IFNα at a dosage of 1.5 mg IFNα-equivalent/kg body weight (n = 8–10, $^{*}P < 0.05$, $^{**}P < 0.01$) once a week 4 times. The arrows represent the time points of injection. (B) Survival of the mice after the treatments (n = 8–10, $^{***}P < 0.001$, considerable difference for IFNα-ELP$_{diblock}$ relative to other groups). (C) H&E staining of tumor after the treatments.

the circulation time and enhance the retention in the tumor. When the intratumoral micelle concentration is below the CMC, the micelles can disintegrate to release IFNα-ELP(A)48-ELP(I)48 unimers with recovered activity and reduced size for tumor penetration, leading to the substantially improved in vivo antitumor efficacy. The enhanced antitumor activity of IFNα-ELP$_{diblock}$ was further corroborated by hematoxylin and eosin (H&E) staining of tumor tissues after the treatments, as implied by a more extensive cell apoptosis observed in the IFNα-ELP$_{diblock}$ treatment (Fig. 5C). Collectively, these results demonstrate that IFNα-ELP$_{diblock}$ was much more efficient than IFNα-ELP(A) and even better than PEGASYS in antitumor efficacy.

3.6. Biosafety study

The biosafety of IFNα-ELP$_{diblock}$ was further studied after the treatment. No considerable loss of mouse body weight was measured for all of the treatments (Fig. 6A). No detectable histological alterations in major organs such as lung, kidney, heart, liver, and spleen were observed for all the drug treatments relative to the saline treatment (Fig. 6B), indicating that all the drug treatments at the same dose did not damage the major organs significantly. These results were corroborated by blood biochemsitry analysis (Fig. 6C), showing that the levels of the functional markers for liver, heart, and kidney fluctuated within the normal ranges, indicating that all the drug treatments did not induce obvious toxicity to liver, heart, and kidney. Hematological examination showed that the levels of the major hematological parameters changed within the normal ranges (Fig. 6D), implicating that all the drug treatments did not result in significant hematological toxicity. All of the biosafety data indicate that all the drug treatments in this study did not induce detectable systemic toxicity.

4. Conclusions

In summary, we have demonstrated TISA of IFNα-ELP$_{diblock}$ into a micelle that is distinguishable, in structure and function, from IFNα-ELP(A) and PEGASYS. First, in response to the body temperature, IFNα-ELP$_{diblock}$ can self-assemble into a uniform spherical micelle with well-retained bioactivity as compared to PEGASYS. Second, the micelle is highly stable in structure and function against proteolysis, presumably due to the close packing of the IFNα-ELP(A)48 block in the corona of the micelle. Third, as a result of the enlarged size and improved stability of the micelle, the half-life of IFNα-ELP$_{diblock}$ is much longer than those of IFNα-ELP(A), IFNα, and even PEGASYS. Fourth, IFNα-ELP$_{diblock}$ can efficiently accumulate into tumors as compared to IFNα-ELP(A), IFNα, and even PEGASYS. Fifth, as a result of the improved pharmacokinetics and tumor retention, IFNα-ELP$_{diblock}$ is much more effective in suppressing tumor growth than IFNα, IFNα-ELP(A) and even PEGASYS at the same dose in a nude mouse model of ovarian tumor, along with a considerably increased animal survival rate (40%) for IFNα-ELP$_{diblock}$ as compared to those for IFNα (0%), IFNα-ELP(A) (0%) and even PEGASYS (10%). In our previous work, we reported that an IFNα-amphiphilic diblock copolymer conjugate without thermo-sensitivity can self-assemble into micelles during the site-specific in situ polymerization [17]. The micelles can elongate the circulation half-life of IFNα and enhance the treatment effect, but the amphiphilic diblock copolymer is not precisely-defined in structure and biodegradable, and the chemical synthesis of the micelles is cumbersome. In contrast, in this work, ELP$_{diblock}$ is precisely-defined in structure and function, biocompatible, biodegradable, and thermosensitive. Moreover, IFNα-ELP$_{diblock}$ can be genetically designed, easily biosynthesized and purified. Taken together, these advantages make IFNα-ELP$_{diblock}$ interesting as a new, long-acting and potent biologic for the treatments of cancer and potentially hepatitis. We speculate that the strategy of TISA is applicable to other therapeutic proteins to significantly improve their stability and pharmacology.

Declaration of Competing Interest

The authors declare no competing financial interest.

Acknowledgements

This work was funded by the National Natural Science Foundation of China (Grant No. 21534006), China Postdoctoral Science Foundation (Grant No. 2019M660826) and Fundamental Research Funds for the Central Universities. The Laboratory Animal Facility is accredited by the AAALAC (Association for Assessment and Accreditation of Laboratory Animal Care International), and all animal protocols used in this study are approved by the Institutional Animal Care and Use

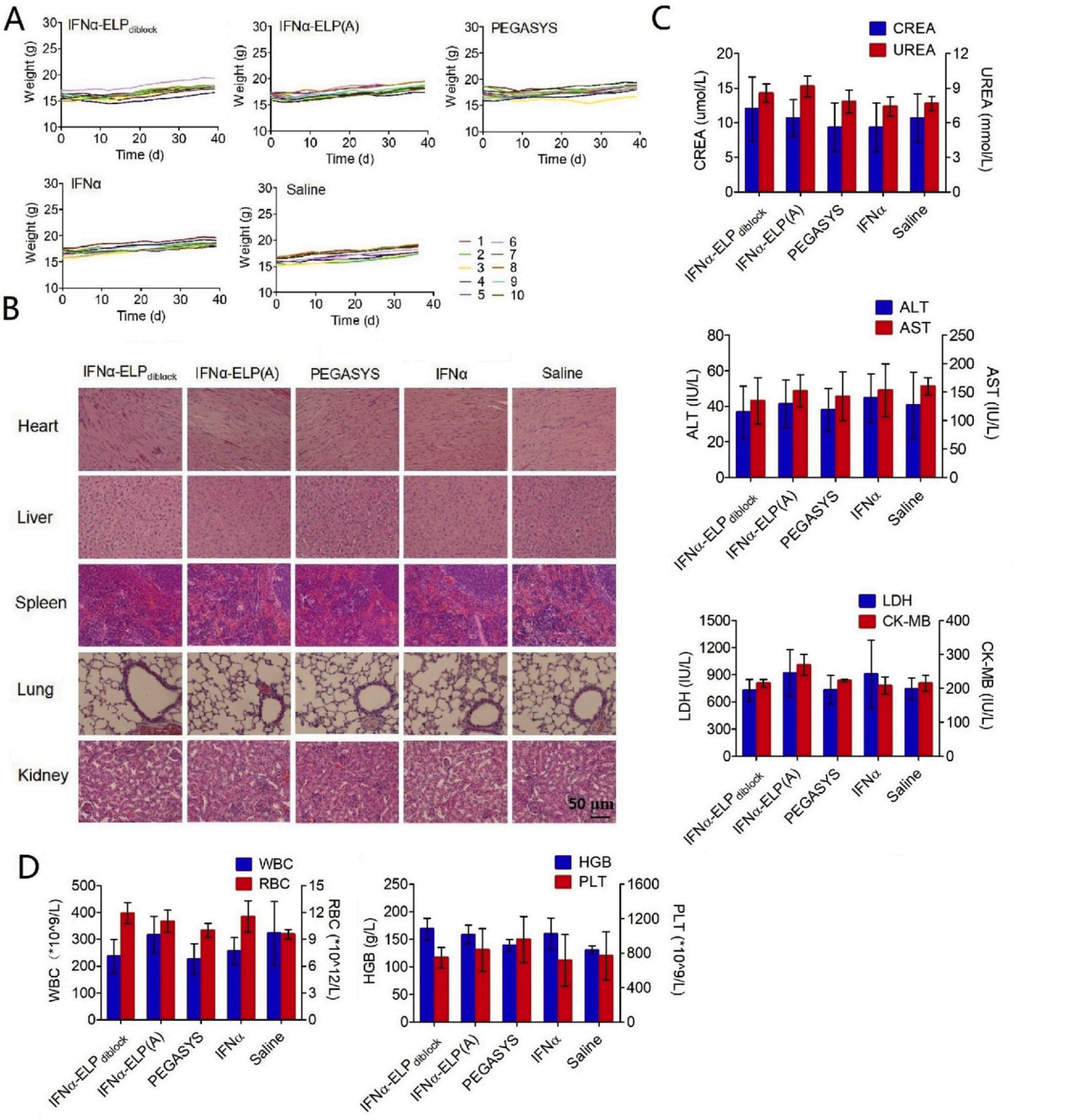

Fig. 6. Biosafety of IFNα-ELP$_{diblock}$. (A) The change of mouse body weight post administration of IFNα-ELP$_{diblock}$, IFNα-ELP(A), PEGASYS, IFNα or Saline (n = 8–10). (B) H&E staining of major tissues after the treatments. (C) Biochemistry examinations for the mice post administration of IFNα-ELP$_{diblock}$, IFNα-ELP(A) or IFNα. Kidney function markers: blood urea nitrogen (UREA); creatinine (CREA). Liver function markers: aspartate aminotransferase (AST); alanine aminotransferase (ALT). Heart function markers: creatine kinase isoenzymes (CK-MB); lactate dehydrogenase (LDH), (n = 3). (D) Hematological examinations for the mice post administration of IFNα-ELP$_{diblock}$, IFNα-ELP(A) or IFNα. Red blood cells (RBC); white blood cells (WBC); platelets (PLT); hemoglobin (HGB) (n = 3). (For interpretation of the references to colour in this figure legend, the reader is referred to the web version of this article.)

Committee (IACUC).

Appendix A. Supplementary data

Supplementary data to this article can be found online at https://doi.org/10.1016/j.jconrel.2020.08.065.

References

[1] B. Leader, Q.J. Baca, D.E. Golan, Protein therapeutics: a summary and pharmacological classification, Nat. Rev. Drug Discov. 7 (2008) 21–39.
[2] G. Walsh, Biopharmaceutical benchmarks 2010, Nat. Biotechnol. 28 (2010) 917–924.
[3] R.J. Wills, Clinical pharmacokinetics of interferons, Clin. Pharmacokinet. 19 (1990) 390–399.
[4] S.D. Putney, P.A.A. Burke, Improving protein therapeutics with sustained release formulations, Nat. Biotechnol. 16 (1998) 153–157.
[5] F.M. Veronese, Peptide and protein PEGylation: a review of problems and solutions, Biomaterials 22 (2001) 405–417.
[6] M.J. Roberts, M.D. Bentley, J.M. Harris, Chemistry for peptide and protein PEGylation, Adv. Drug Deliv. Rev. 54 (2002) 459–476.
[7] J.M. Harris, R.B. Chess, Effect of pegylation on pharmaceuticals, Nat. Rev. Drug Discov. 2 (2003) 214–221.

[8] W. Zhao, F. Liu, Y. Chen, J. Bai, W. Gao, Synthesis of well-defined protein-polymer conjugates for biomedicine, Polymer 66 (2015) A1–A10.
[9] X. Liu, J. Sun, W. Gao, Site-selective protein modification with polymers for advanced biomedical applications, Biomaterials 178 (2018) 413–434.
[10] F. Zhang, M. Liu, H. Wan, Discussion about several potential drawbacks of PEGylated therapeutic proteins, Biol. Pharm. Bull. 37 (2014) 335–339.
[11] V. Schellenberger, C.W. Wang, N.C. Geething, B.J. Spink, A. Campbell, W. To, M.D. Scholle, Y. Yin, Y. Yao, O. Bogin, J.L. Cleland, J. Silverman, W.P. Stemmer, A recombinant polypeptide extends the in vivo half-life of peptides and proteins in a tunable manner, Nat. Biotechnol. 27 (2009) 1186–1190.
[12] M. Schlapschy, U. Binder, C. Borger, I. Theobald, K. Wachinger, S. Kisling, D. Haller, A. Skerra, PASylation: a biological alternative to PEGylation for extending the plasma half-life of pharmaceutically active proteins, A. Protein Eng. Des. Sel. 26 (2013) 489–501.
[13] J. Hu, G. Wang, X. Liu, W. Gao, Enhancing pharmacokinetics, tumour retention, and antitumour efficacy by elastin-like polypeptide fusion of interferon alpha, Adv. Mater. 27 (2015) 7320–7324.
[14] Y. Hou, Y. Zhou, H. Wang, R. Wang, J. Yuan, Y. Hu, K. Sheng, J. Feng, S. Yang, H. Lu, Macrocyclization of interferonepoly (a-amino acid) conjugates significantly improves the tumour retention, penetration, and antitumour efficacy, J. Am. Chem. Soc. 140 (2018) 1170e1178.
[15] J. Hu, G. Wang, W. Zhao, X. Liu, L. Zhang, W. Gao, Site-specific in situ growth of an interferon-polymer conjugate that outperforms PEGASYS in cancer therapy, Biomaterials 96 (2016) 84e92.
[16] J. Hu, G. Wang, W. Zhao, W. Gao, In situ growth of a C-terminal interferon-alpha conjugate of a phospholipid polymer that outperforms PEGASYS in cancer therapy, J. Control. Release 237 (2016) 71–77.
[17] X. Liu, M. Sun, J. Sun, J. Hu, Z. Wang, J. Guo, W. Gao, Polymerization induced self-assembly of a site-specific interferon α-block copolymer conjugate into micelles with remarkably enhanced pharmacology, J. Am. Chem. Soc. 140 (2018) 10435–10438.
[18] L.M. Pfeffer, C.A. Dinarello, R.B. Herberman, B.R. Williams, E.C. Borden, R. Bordens, W.R. Walter, T.L. Nagabhushan, P.P. Trotta, S. Pestka, Biological properties of recombinant α-interferons: 40th anniversary of the discovery of interferons, Cancer Res. 58 (1998) 2489–2499.
[19] L. Zitvogel, L. Galluzzil, O. Kepp, M.J. Smyth, G. Kroemer, Type I interferons in anticancer immunity, Nat. Rev. Immunol. 15 (2015) 405–414.
[20] D.W. Urry, T.M. Parker, M.C. Reid, D.C. Gowda, Biocompatibility of the bioelastic materials, poly(Gvgvp) and its gamma-irradiation cross-linked matrix - summary of generic biological test-results, J. Bioactive Comp. Polym. 6 (1991) 263–282.
[21] D.W. Urry, Physical chemistry of biological free energy transduction as demonstrated by elastic protein-based polymers, J. Phys. Chem. B 101 (1997) 11007–11028.
[22] D.E. Meyer, A. Chilkoti, Quantification of the effects of chain length and concentration on the thermal behaviour of elastin-like polypeptides, Proc. Biomacromolecules 5 (2004) 846–851.
[23] D.W. Urry, C.-H. Luan, T.M. Parker, Temperature of polypeptide inverse temperature transition depends on mean residue hydrophobicity, J. Am. Chem. Soc. 113 (1991) 4346–4348.
[24] F. Sciortino, D.W. Urry, M.U. Palma, K.U. Prasad, Self-assembly of a bioelastomeric structure: solution dynamics and the spinodal and coacervation lines, Biopolymers 277 (2018) 1401–1407.
[25] D.W. Urry, D.C. Gowda, T.M. Parker, C.H. Luan, M.C. Reid, C.M. Harris, A. Pattanaik, R.D. Harris, Hydrophobicity scale for proteins based on inverse temperature transitions, Biopolymers 32 (1992) 1243–1250.
[26] D.W. Urry, T.L. Trapane, K.U. Prasad, Phase-structure transitions of the elastin polypentapeptide-water system within the framework of composition-temperature studies, Biopolymers 24 (1985) 2345–2356.
[27] M.R. Dreher, A.J. Simnick, K. Fischer, R.J. Smith, A. Patel, M. Schmidt, A. Chilkoti, Temperature triggered self-assembly of polypeptides into multivalent spherical micelles, J. Am. Chem. Soc. 130 (2008) 687–694.
[28] Y. Gao, G. Yu, Y. Wang, C. Dang, T.C. Sum, H. Sun, H.V. Demir, Full color emission from II-VI semiconductor quantum dot-polymer composites, J. Phys. Chem. Lett. 7 (2016) 2772–2778.
[29] R.E. Sallach, M. Wei, N. Biswas, V.P. Conticello, S. Lecommandoux, R.A. Dluhy, E.L. Chaikof, Micelle density regulated by a reversible switch of protein secondary structure, J. Am. Chem. Soc. 128 (2006) 12014–12019.
[30] W. Kim, J. Thevenot, E. Ibarboure, S. Lecommandoux, E.L. Chaikof, Self-assembly of thermally responsive amphiphilic diblock copolypeptides into spherical micellar nanoparticles, Angew. Chem. Int. Ed. Eng. 49 (2010) 4257–4260.
[31] O.S. Rabotyagova, P. Cebe, D.L. Kaplan, Protein-based block copolymers, Biomacromolecules 12 (2011) 269–289.
[32] W. Hassouneh, E.B. Zhulina, A. Chilkoti, M. Rubinstein, Elastin-like polypeptide diblock copolymers self-assemble into weak micelles, Macromolecules 48 (2015) 4183–4195.
[33] K. Widder, S.R. MacEwan, E. Garanger, V. Nunez, S. Lecommandoux, A. Chilkoti, D. Hinderberger, Structural evolution of a stimulus-responsive diblock polypeptide micelle by temperature tunable compaction of its core, Soft Matter 13 (2017) 1816–1822.
[34] A.J. Simnick, C.A. Valencia, R. Liu, A. Chilkoti, Morphing low-affinity ligands into high-avidity nanoparticles by thermally triggered self-assembly of a genetically encoded polymer, ACS Nano 4 (2010) 2217–2227.
[35] J. Wang, M. Dzuricky, A. Chilkoti, The weak link: optimization of the ligand-nanoparticle interface to enhance cancer cell targeting by polymer micelles, Nano Lett. 17 (2017) 5995–6005.
[36] J. Wang, J. Min, S.A. Eghtesadi, R.S. Kane, A. Chilkoti, A quantitative study of the interaction of multivalent ligand-modified nanoparticles with breast cancer cells with tunable receptor density, ACS Nano 14 (2020) 372–383.
[37] Z. Wang, J. Guo, J. Ning, X. Feng, X. Liu, J. Sun, X. Chen, F. Lu, W. Gao, One-month zero-order sustained release and tumor eradication after a single subcutaneous injection of interferon alpha fused with a body-temperature-responsive polypeptide, Biomater. Sci. 7 (2018) 104–112.
[38] J.R. McDaniel, J.A. MacKay, F.C. Quiroz, A. Chilkoti, Recursive directional ligation by plasmid reconstruction allows rapid and seamless cloning of oligomeric genes, Biomacromolecules 11 (2010) 944–952.
[39] W. Burchard, M. Schmidt, W.H. Stockmayer, Information on polydispersity and branching from combined quasielastic and intergrated scattering, Macromolecules 13 (1980) 1265–1272.
[40] X. Liu, W. Gao, Precision conjugation: an emerging tool for generating protein-polymer conjugates, Angew. Chem. Int. Ed. (2020), https://doi.org/10.1002/anie.202003708.
[41] N.A. de Weerd, T. Nguyen, The interferons and their receptors-distribution and regulation, Immunol. Cell Biol. 90 (2012) 483–491.